Comparison of Five Depth-Averaged 2-D Turbulence Models for River Flows

Weiming Wu, Pingyi Wang and Nobuyuki Chiba
National Center for Computational Hydroscience and Engineering
The University of Mississippi, MS 38677

Abstract: In this study, five depth-averaged 2-D turbulence models for river flows, including the depth-averaged parabolic eddy viscosity model, modified mixing length model, standard k-ε turbulence model, non-equilibrium k-ε turbulence model and re-normalized group (RNG) k-ε turbulence model, are compared in the simulation of flows around a spur-dyke, in a sudden-expanded flume and in two natural rivers. It is shown that in the two field cases where the channel geometries are simple, all five models can give generally good predictions for the main flow features. However, in the two laboratory cases where the channel geometries are complex, differences have been found among these models. The depth-averaged parabolic eddy viscosity model over-predicts the recirculation flows behind the spur-dyke and the flume expansion. The modified mixing length model gives better prediction than the depth-averaged parabolic model. The standard k-ε turbulence model predicts well for the recirculation flow in the sudden-expended flume but under-predicts the length of recirculation zone behind the spur-dyke, while the non-equilibrium and RNG k-ε turbulence models provide good results for both laboratory cases.

Keywords: Turbulence Model; Depth-Averaged Two-dimensional Model; River Flow; Zero-Equation Turbulence Model; k-ε Turbulence Model.

1. INTRODUCTION

Many turbulence models based on Reynolds-averaged Navier-Stokes equations, such as zero-equation turbulence model, one-equation turbulence model, two-equation turbulence model and Reynolds stress/flux model, have been successfully applied to the simulation of turbulent flows in computational fluid dynamics (CFD). In recent years, the large eddy simulation and direct numerical simulation of turbulent flows have also been progressed remarkably. These turbulence modeling techniques have been gradually applied in the simulation of river flows. However, because the computational domain in natural rivers is very irregular and even movable, the simulation of turbulent flow in rivers is less developed and mostly stays in the level of two-equation turbulence models or simpler ones. For the depth-averaged simulation of river flows, one of the most often used two-equation turbulence models is Rastogi and Rodi's (1978) depth-averaged standard k-ε turbulence model. In the present study, Chen and Kim's (1987) non-equilibrium k-ε turbulence model and Yahkot et al.'s (1992) RNG k-ε turbulence model, which are widely used in CFD, are extended to the depth-averaged 2-D simulation of river flows. These two k-ε turbulence models are compared with other three depth-averaged turbulence models: the depth-averaged parabolic eddy viscosity model, the modified mixing length model, and Rastogi and Rodi's depth-averaged standard k-ε model.

2. GOVERNING EQUATIONS

The depth-integrated continuity and momentum equations of turbulent flow in rivers are:

$$\frac{\partial h}{\partial t}+\frac{\partial(hU)}{\partial x}+\frac{\partial(hV)}{\partial y}=0 \tag{1}$$

$$\frac{\partial(hU)}{\partial t}+\frac{\partial(hUU)}{\partial x}+\frac{\partial(hVU)}{\partial y}=-gh\frac{\partial z_s}{\partial x}+\frac{1}{\rho}\frac{\partial(hT_{xx})}{\partial x}+\frac{1}{\rho}\frac{\partial(hT_{xy})}{\partial y}-\frac{\tau_{bx}}{\rho} \tag{2}$$

$$\frac{\partial(hV)}{\partial t}+\frac{\partial(hUV)}{\partial x}+\frac{\partial(hVV)}{\partial y}=-gh\frac{\partial z_s}{\partial y}+\frac{1}{\rho}\frac{\partial(hT_{yx})}{\partial x}+\frac{1}{\rho}\frac{\partial(hT_{yy})}{\partial y}-\frac{\tau_{by}}{\rho} \tag{3}$$

where t is the time; x and y are the horizontal Cartesian coordinates; h is the flow depth; U and V are the depth-averaged flow velocities in x- and y-directions; z_s is the water surface elevation; g is the gravitational acceleration; ρ is the density of flow; T_{xx}, T_{xy}, T_{yx} and T_{yy} are the depth-averaged turbulent stresses; τ_{bx} and τ_{by} are the bed shear stresses that are determined by $\tau_{bx}=\rho c_f U\sqrt{U^2+V^2}$ and $\tau_{by}=\rho c_f V\sqrt{U^2+V^2}$, in which $c_f=gn^2/h^{1/3}$ and n is the Manning's roughness coefficient.

It should be noted that Eqs. (2) and (3) do not include the dispersion terms that exist due to the vertical nonuniformity of flow velocity. Their effect is assumed to be negligible in this study, but the treatment of these terms has been studied by Flokstra (1977), Wu and Wang (2004) and others.

The turbulent stresses are determined by Boussinesq's assumption

$$T_{xx}=2\rho(v+v_t)\frac{\partial U}{\partial x}-\frac{2}{3}\rho k \tag{4a}$$

$$T_{xy}=T_{yx}=\rho(v+v_t)\left(\frac{\partial U}{\partial y}+\frac{\partial V}{\partial x}\right) \tag{4b}$$

$$T_{yy}=2\rho(v+v_t)\frac{\partial V}{\partial y}-\frac{2}{3}\rho k \tag{4c}$$

where v is the kinematic viscosity of water; v_t is the eddy viscosity due to turbulence; k is the turbulence energy. The k in Eqs. (4a) and (4c) is dropped when the zero-equation turbulence models are considered.

3. TURBULENCE MODELS FOR EDDY VISCOSITY

3.1. Depth-Averaged Parabolic Eddy Viscosity Model

Averaging the eddy viscosity, which approximately yields a parabolic profile, over the flow depth, one can obtain the depth-averaged parabolic model for the eddy viscosity:

$$v_t=\alpha_t U_* h \tag{5}$$

where U_* is the bed shear velocity, $U_* = \left[c_f \left(U^2 + V^2 \right) \right]^{1/2}$; and α_t is an empirical coefficient. Theoretically, α_t should be equal to $\kappa/6$, with κ being the van Karman's constant. However, different values have been given to α_t, which may be due to the anisotropic features of turbulence structures in horizontal and vertical directions. It is commonly accepted that α_t is related to the ratio of channel width and flow depth, having values between $0.3 \sim 1.0$ (Elder, 1959; Fischer et al., 1979).

3.2. Modified Mixing Length Model

Eq. (5) is very simple. It is applicable in the region of main flow, but it does not account for the influence of the horizontal gradient of velocity. Significant errors may exist when it is applied in the region close to rigid walls. Improvement can be achieved through the combination of Eq. (5) and Prandtl's mixing length theory, which reads:

$$\nu_t = \sqrt{ \left(\alpha_0 U_* h \right)^2 + \left(l_h^2 \left| \overline{S} \right| \right)^2 } \tag{6}$$

where $\left| \overline{S} \right| = \left[2\left(\partial U / \partial x \right)^2 + 2\left(\partial V / \partial y \right)^2 + \left(\partial U / \partial y + \partial V / \partial x \right)^2 \right]^{1/2}$; α_0 is an empirical coefficient, set as $\kappa/6$; l_h is the horizontal mixing length, and is determined by $l_h = \kappa \min \left(c_m h, y \right)$, with y being the distance to the nearest wall, and c_m being an empirical coefficient.

3.3. Standard k-ε Turbulence Model

Rastogi and Rodi (1978) established the depth-averaged k-ε turbulence model through depth-integrating the 3-D standard k-ε model. The eddy viscosity ν_t is calculated by

$$\nu_t = c_\mu k^2 / \varepsilon \tag{7}$$

where c_μ is an empirical constant. The turbulence energy k and its dissipation rate ε are determined with the following model transport equations:

$$\frac{\partial k}{\partial t} + U \frac{\partial k}{\partial x} + V \frac{\partial k}{\partial y} = \frac{\partial}{\partial x} \left(\frac{\nu_t}{\sigma_k} \frac{\partial k}{\partial x} \right) + \frac{\partial}{\partial y} \left(\frac{\nu_t}{\sigma_k} \frac{\partial k}{\partial y} \right) + P_h + P_{kv} - \varepsilon \tag{8}$$

$$\frac{\partial \varepsilon}{\partial t} + U \frac{\partial \varepsilon}{\partial x} + V \frac{\partial \varepsilon}{\partial y} = \frac{\partial}{\partial x} \left(\frac{\nu_t}{\sigma_\varepsilon} \frac{\partial \varepsilon}{\partial x} \right) + \frac{\partial}{\partial y} \left(\frac{\nu_t}{\sigma_\varepsilon} \frac{\partial \varepsilon}{\partial y} \right) + c_{\varepsilon 1} \frac{\varepsilon}{k} P_h + P_{\varepsilon v} - c_{\varepsilon 2} \frac{\varepsilon^2}{k} \tag{9}$$

where $P_h = \nu_t \left| \overline{S} \right|^2$; $P_{kv} = c_f^{-1/2} U_*^3 / h$; $P_{\varepsilon v} = c_{\varepsilon\Gamma} c_{\varepsilon 2} c_\mu^{1/2} c_f^{-3/4} U_*^4 / h^2$; $c_{\varepsilon 1}$, $c_{\varepsilon 2}$, $c_{\varepsilon\Gamma}$, σ_k and σ_ε are empirical coefficients. The standard values of these coefficients are: $c_\mu = 0.09$, $c_{\varepsilon 1} = 1.44$, $c_{\varepsilon 2} = 1.92$, $\sigma_k = 1.0$, $\sigma_\varepsilon = 1.3$, and $c_{\varepsilon\Gamma} = 1.8 - 3.6$.

3.4. Non-equilibrium k-ε Turbulence Model

Chen and Kim (1987) modified the standard k-ε turbulence model to consider the non-equilibrium between the generation and dissipation of turbulence. A second time scale of the production range of turbulence kinetic energy spectrum is added to the dissipation rate equation,

which results in a functional form of coefficient $c_{\varepsilon 1}$ as $c_{\varepsilon 1} = 1.15 + 0.25 P_h / \varepsilon$. The other parameters are $c_\mu = 0.09$, $c_{\varepsilon 2} = 1.90$, $\sigma_k = 0.8927$, and $\sigma_\varepsilon = 1.15$. The modified model was called the non-equilibrium k-ε turbulence model (Shyy et al., 1997), which has been tested in a compressible recirculating flow with improved performance over the standard model. By using Rastogi and Rodi's (1978) depth-averaging approach, the depth-averaged non-equilibrium k-ε model can be derived from the 3-D version. The formulations of k- and ε-equations are still the same as Eqs. (8) and (9), with only the model coefficients being replaced accordingly.

3.5. RNG k-ε Turbulence Model

Yakhot et al. (1992) re-derived the ε-equation (9) using the re-normalized group (RNG) theory. One new term was introduced to take into account the highly anisotropic features, usually associated with regions of large shear, and to modify the viscosity accordingly. This term was claimed to improve the simulation accuracy of the RNG k-ε turbulence model for highly strained flow. In analogy to the above non-equilibrium turbulence model, the depth-averaged 2-D RNG k-ε turbulence model can also be derived, whose k- and ε-equations are the same as Eqs. (8) and (9), with the new term being included in the coefficient $c_{\varepsilon 1}$ as $c_{\varepsilon 1} = 1.42 - \eta\left(1 - \eta/\eta_0\right)/\left(1 + \beta\eta^3\right)$. Here, $\beta = 0.015$, $\eta = \left|\overline{S}\right| k / \varepsilon$, and $\eta_0 = 4.38$. The other coefficients are $c_\mu = 0.085$, $c_{\varepsilon 2} = 1.68$, $\sigma_k = 0.7179$, and $\sigma_\varepsilon = 0.7179$.

4. BOUNDARY CONDITIONS

Near rigid wall boundaries, such as banks and islands, the wall-function approach is employed. By applying the log-law of velocity, the resultant wall shear stress $\vec{\tau}_w$ is related to the flow velocity $\vec{V}_P$ at the center P of the control volume close to the wall by the following relation:

$$\vec{\tau}_w = -\lambda \vec{V}_P \tag{10}$$

where λ is a coefficient. In the k-ε turbulence models, λ is determined by $\lambda = \rho c_\mu^{1/4} k_P^{1/2} \kappa / \ln\left(E y_P^+\right)$, which is valid in the range of $11.6 < y_P^+ < 300$. Here, $y_P^+ = \rho c_\mu^{1/4} k_P^{1/2} y_P / \mu$. It should be noted that in the derivation of λ, the relation $u_* = c_\mu^{1/4} k_P^{1/2}$ is used, which can be obtained with the assumption of local equilibrium of turbulence (see Rodi, 1993). In the zero-equation turbulence models, the turbulence energy k is not solved, and hence λ is determined by $\lambda = \rho u_* \kappa / \ln\left(E y_P^+\right)$ with $y_P^+ = \rho u_* y_P / \mu$ instead.

In three k-ε turbulence models, the turbulence generation P_h and the dissipation rate near the wall are determined by $P_{h,P} = \tau_w^2 / \kappa \mu y_P^+$ and $\varepsilon_P = c_\mu^{3/4} k_P^{3/2} / \kappa y_P$.

In the simulation of the flow in an open channel with sloped banks, sand bars and islands, the computational domain may be partly wet or dry due to the water surface change. In the present model, a threshold flow depth (a small value such as 0.02m in natural rivers) is used to judge drying and wetting. If the flow depth in a node is larger than the threshold value, this node

is considered to be wet, and if the flow depth is lower than the threshold value, this node is dry. The above wall-function approach is applied in the water edge between the wet and dry nodes.

5. NUMERICAL METHODS

The above turbulence models are implemented in the depth-averaged 2-D model for shallow water flow in open channels developed by Wu (2004) on the basis of the general 2-D flow model of Zhu (1992). The governing equations are discretized using the finite volume method on a curvilinear, non-staggered grid. The convection terms are discretized by the HLPA scheme (Zhu, 1991). The diffusion terms are discretized by the central difference scheme. The pressure and velocity coupling is achieved by using SIMPLEC algorithm with Rhie and Chow's (1983) momentum interpolation technique. The resulting algebraic equations are solved by Stone's (1968) strongly implicit procedure (SIP). The details of numerical methods can be found in Wu (2004).

6. SIMULATION RESULTS

Case 1: Flow around a Spur-Dyke

Rajaratnam and Nwachukwu (1983) measured the flow around a spur-dyke. The experiments were conducted in a straight tilting rectangular flume, 37 m long, 0.92 m wide and 0.76 m deep. The experimental run A1 is simulated here. The flume bed and walls were smooth, and the spur-dyke used in this case was an aluminum plate with a thickness of 3 mm and a projection length of 0.152 m. The flow discharge was 0.0453 m^3/s, and the approach flow depth was 0.189 m. The computational mesh consists of 103×32 nodes in longitudinal and transverse directions, part of which around the spur-dyke is shown in Fig. 1.

Fig. 2 shows the flow patterns calculated by using these five turbulence models, and Fig. 3 shows the comparison of the measured and calculated flow velocities in cross sections located at x/b=2, 4, 6 and 8. Here, b is the length of the spur-dyke. The coefficient α_t in the depth-averaged parabolic model is given as 1.0. $c_m = 0.4$ is used in the modified mixing length model. $c_{\varepsilon\Gamma} = 3.6$ is used for all three k-ε turbulence models. All five turbulence models reasonably predict the main flow around the spur-dyke. However, the recirculation flows simulated by the five models do have significant differences. The depth-averaged parabolic model over-predicts the strength of the backward flow near the wall around the cross section of x/b=6. The modified mixing length model provides a better prediction for the velocity than the depth-averaged parabolic model. The standard k-ε turbulence model under-predicts the length of the recirculation zone. The results of the non-equilibrium and RANG k-ε turbulence models are very close to each other, and better than the results from the standard k-ε model.

Fig. 4 shows the contours of eddy viscosities calculated by five turbulence models. The patterns of the viscosity contours from three k-ε turbulence models are very similar. The eddy viscosity calculated by the non-equilibrium and RNG k-ε turbulence models are very close to each other, but the eddy viscosity by the standard k-ε turbulence model is larger. The eddy viscosity by the depth-averaged parabolic model has larger values in the main flow than those

calculated by the other four models, while the modified mixing length model gives very large eddy viscosity around the tip of the spur-dyke.

Case 2: Flow in a Sudden-Expanded Flume

The flow in a sudden-expanded flume was measured by Xie (1996) and her colleagues. The experiment was conducted in a cement-coated flume, with a length of 18m, a width of 1.2m and a slope of 1/1000. Half of the flume width in the upper part was blocked, forming an expansion of the flume width from 0.6m to 1.2m at the location of 7.7m from the entrance. The flow discharges were 0.01815 m^3/s and 0.03854 m^3/s in two experimental runs. The computational mesh has 121×36 nodes, part of which around the expansion is shown in Fig. 5. Figs. 6 and 7 show the comparisons of the measured and calculated depth-averaged velocity profiles along six cross sections in two experimental runs. The non-equilibrium and RNG k-ε models provide generally good results. They perform the same in this case and the previous spur-dyke case, with the same coefficients being used. The standard k-ε model also provides good predictions in this case. The depth-averaged parabolic model still over-predicts the strength of the backward flow in the recirculation zone. The modified mixing length model gives better prediction than the depth-averaged parabolic model, after its empirical coefficient c_m is adjusted to 1.1.

Case 3: Flow in the Fall River

The Fall River is located in Rocky Mountain National Park, Colorado. The study reach was about 100 m long, consisting of two opposite bends. The radius of curvature of the first and second bends was 11.0 m and 13.5 m, respectively. The channel width at bankfull stage was about 9 m (Thorne et al., 1985). The river was covered with coarse sand. The flow discharge was 4 m^3/s, which was at bankfull stage. The water surface level at the outlet was 2.61 m. Fig. 8 shows the river planform and the computational mesh.

In this case, the coefficient α_t in the depth-averaged parabolic model is given as 0.6. c_m in the modified mixing length model is specified as 1.2. The $c_{\varepsilon\Gamma}$ in three k-ε turbulence models is set as 1.8. Fig. 9 shows the flow pattern calculated by using the standard k-ε turbulence model. The main flow is specified along the left bank in the entrance, and it does not change in the first bend and in the transitional stretch, but it turns to the right bank (outer bank) in the second bend just at about the bend apex. Two recirculation zones are produced. A very small one is in the transitional stretch, and a bigger one locates behind the apex along the inner bank of the second bend. The flow patterns calculated by using other four turbulence models are similar to that shown in Fig. 9. All five turbulence models capture the major features of the flow.

Fig. 10 shows the comparison of the eddy viscosities along the cross section CS-5A calculated by the five turbulence models. The eddy viscosities calculated by the three k-ε models are very close to each other, but significant differences are found among the k-ε models and the zero-equation turbulence models. Fig. 11 shows the comparison of the measured and calculated flow velocities in six cross sections. Because the convection is dominant in this case, even though the eddy viscosities calculated by the five turbulence models are obviously different, the velocities predicted by using the five models are close to each other. All the simulated velocities agree reasonably well with the measured values.

It should be noted that a relatively coarse mesh is used in the simulation. This is due to the consideration that the flow in a natural river is simulated. In order to investigate the influence of mesh size, a refined mesh is also used. This refined mesh is obtained from the coarse mesh by adding one node between each two nodes in longitudinal and transverse directions. However, the flow patterns and velocities calculated using these two meshes do not have significant difference.

Case 4. Flow in the Dommel River

The study reach in the Dommel River in the Netherlands is 285m long, containing two opposite bends of almost 90°, with a short straight reach in between and long straight reaches upstream and downstream. The channel width is almost constant, approximately 8m at bankfull stage. Fig. 12 shows the computational mesh consisting of 151×26 nodes. The flow discharge is 1.4 m^3/s, and the water elevation at the outlet is 26.55m. The flow was measured by de Vriend and Geldof (1983).

Fig. 13 shows the flow pattern through the two bends calculated by the standard k-ε turbulence model. The flow occurs in the central part while the blank parts along two banks are dry zones. Other four models give very similar results. Fig. 14 shows the comparison of the measured and calculated depth-averaged velocities in six cross sections whose locations are shown in Fig. 12. The coefficients of the five models in this case are the same as those used in the case of the Fall River, as presented in Table 1. Again, the velocities predicted by the five models are very close to each other, with reasonable agreement with the measured data.

7. CONCLUSIONS

Two zero-equation turbulence models and three k-ε turbulence models for depth-averaged 2-D river flows have been compared in this study. The two zero-equation turbulence models are the depth-averaged parabolic eddy viscosity model and the modified mixing length model. The three k-ε turbulence models are the Rastogi and Rodi's (1978) depth-averaged 2-D standard k-ε turbulence model as well as the depth-averaged 2-D non-equilibrium and RNG k-ε turbulence models derived from Chen and Kim's (1987) and Yakhot et al.'s (1992) 3-D turbulence models following Rastogi and Rodi's depth-averaging approach.

The comparison in two natural rivers with simple channel geometry shows that the flow velocity distributions predicted by the five turbulence models are very similar. However, the simulated secondary flow features around a spur-dyke and in a sudden-expanded flume calculated by the five turbulence models are found to be obviously different. The depth-averaged parabolic eddy viscosity model over-predicts the strength of the backward flow in the recirculation zone, while the modified mixing length model gives reasonable prediction if its coefficient is adjusted. The standard k-ε turbulence model under-predicts the length of recirculation zone behind the spur-dyke but provides good prediction in the case pf sudden-expanded flume. The non-equilibrium and RNG k-ε turbulence models provide better results for the flow with high shear strain than the standard k-ε turbulence model.

REFERENCES

Chen, Y.-S and Kim, S.-M. (1987). "Computation of turbulent flows using an extended k-ε turbulence closure model." *CR-179204*, NASA, p. 21.

De Vriend, H.J. and Geldof, H.J. (1983). "Main flow velocity in short and sharply curved river bends," *Report No. 83-6*, Delft University of Technology, The Netherlands.

Elder, J.W. (1959). "The dispersion of marked fluid in turbulent shear flow," *J. of Fluid Mechanics*, Vol.5, Part 4.

Fischer, H.B., List, E.J., Koh, R.C.Y., Imberger, J., Brooks, N.H (1979). *Mixing in Inland and Coastal Waters*, Academic Press, New York.

Flokstra, C. (1977). "The closure problem for depth-average two dimensional flow." *Publication No. 190*, Delft Hydraulics Laboratory, The Netherlands.

Rajaratnam, N., and Nwachukwu, B.A. (1983). "Flow near groin-like structures," *J. of Hydraulic Engineering*, 109(3), 463-481.

Rastogi, A.K. and Rodi, W. (1978). "Predictions of heat and mass transfer in open channels." *J. of the Hydraulics Division*, ASCE, 104(3), 397-420.

Rhie, C.M. and Chow, W.L. (1983). "Numerical study of the turbulent flow past an airfoil with trailing edge separation." *AIAA J.*, 21, 1525-1532.

Rodi, W. (1993), *Turbulence Models and Their Application in Hydraulics*, 3rd Ed., IAHR Monograph, Balkema, Rotterdam.

Shyy, W., Thakur, S.S., Quyang, H., Liu, J. and Blosch, E. (1997). *Computational Techniques for Complex Transport Phenomenon*. Cambridge University Press.

Stone, H.L. (1968). "Iterative solution of implicit approximation of multidimensional partial differential equations," *SIAM J. on Numerical Analysis*, 5, 530-558.

Thorne, C.R., Zevenbergen, L.W., Bradley, J.B. and Pitlick, J.C. (1985). "Measurements of bend flow hydraulics of the fall river at bankfull stage." *WRD Project Report No. 85-3*, Water Resources Division, Fort Collins, Colorado.

Wu, W. (2004). "Depth-averaged 2-D numerical modeling of unsteady flow and nonuniform sediment transport in open channels." Tentatively accepted for publication by *J. of Hydraulic Engineering*, ASCE.

Wu, W. and Wang, S. S.Y. (2004). "Depth-averaged 2-D calculation of flow and sediment transport in curved channels." Under review by *Int. J. of Sediment Research*.

Xie, B.L. (1996). "Experiment on flow in a sudden-expanded channel," *Technical Report*, Wuhan University of Hydraulic and Electric Engineering, China.

Yakhot, V., Orszag, S.A., Thangam, S., Gatski, T.B. and Speziale, C.G. (1992). "Development of turbulence models for shear flows by a double expansion technique." *Phys. Fluids A*, 4(7).

Zhu, J. (1991). "A low diffusive and oscillation-free convection scheme." *Communications in applied numerical methods*, Vol. 7.

Zhu, J. (1992). "FAST2D: A computer program for numerical simulation of two-dimensional incompressible flows with complex boundaries." *Report No. 690*, Institute of Hydromechanics, Karlsruhe University.

Table 1. Summary of Model Coefficients used in Test Cases

Test Cases	Depth-Av. Parabolic Model	Modified Mixing Length Model	Standard k-ε Model	Non-equilibrium k-ε Model	RNG k-ε Model
Spur-Dike	α_t=1.0	c_m=0.4	$c_{\varepsilon I}$=3.6	$c_{\varepsilon I}$=3.6	$c_{\varepsilon I}$=3.6
Sudden-Expansion	α_t=1.0	c_m=1.1	$c_{\varepsilon I}$=3.6	$c_{\varepsilon I}$=3.6	$c_{\varepsilon I}$=3.6
Fall River	α_t=0.6	c_m=1.2	$c_{\varepsilon I}$=1.8	$c_{\varepsilon I}$=1.8	$c_{\varepsilon I}$=1.8
Dommel River	α_t=0.6	c_m=1.2	$c_{\varepsilon I}$=1.8	$c_{\varepsilon I}$=1.8	$c_{\varepsilon I}$=1.8

List of Figures

Fig. 1 Computational Mesh around a Spur-Dyke

Depth-Averaged Parabolic Model

Dike   0.2   0.7   1.2   1.7   x (m)

Mixing Length Model

Standard k-ε Model

Non-equilibrium k-ε Model

RNG k-ε Model   0.5m/s
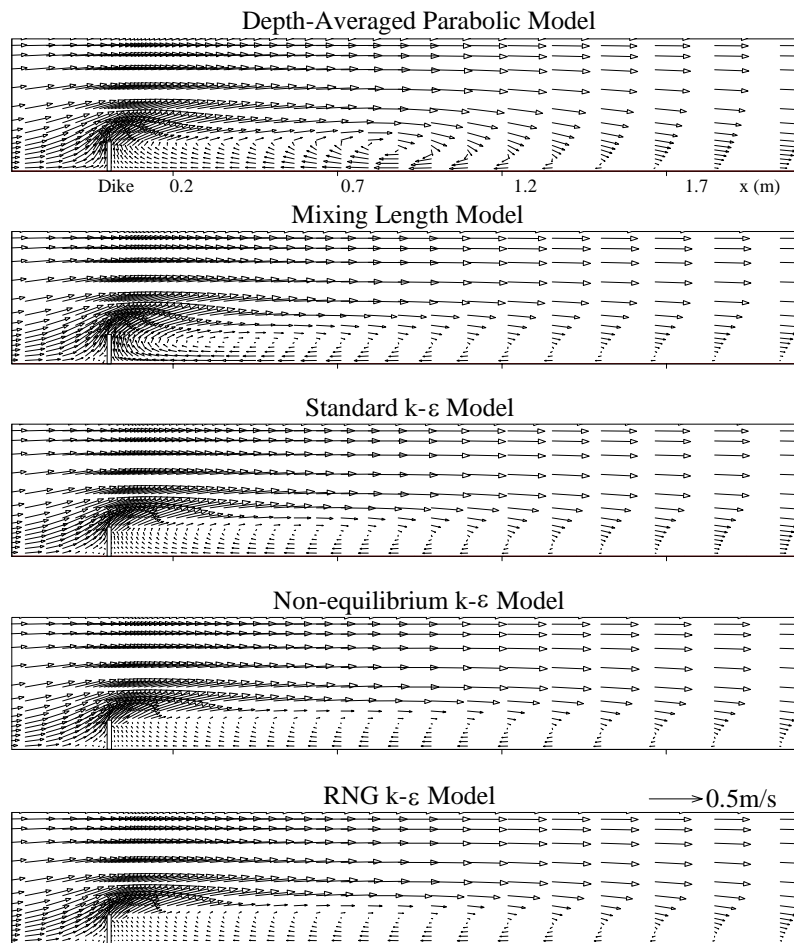
Fig. 2 Simulated Flow Patterns around a Spur-Dyke

13

x/b=2

Distance from Right Wall (m)

DA Parabolic Model
Mixing Length Model
Standard k-ε Model
Non-eq. k-ε Model
RNG k-ε Model
□ Measured

Velocity (m/s)

x/b=4

Distance from Right Wall(m)

Velocity (m/s)

x/b=6

Distance from Right Wall (m)

Velocity (m/s)

x/b=8

Distance from Right Wall (m)

Velocity (m/s)
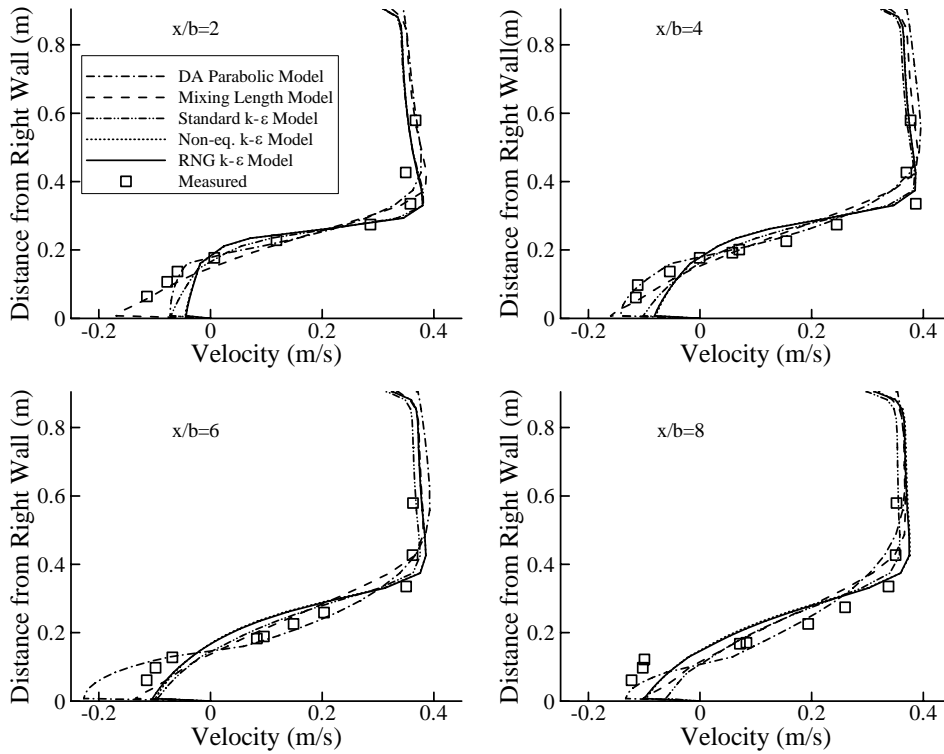
Fig. 3 Measured vs. Calculated Flow Velocities around a Spur-Dyke

Depth-Averaged Parabolic Model

0.0028

0.0034   0.0028

0.0022   0.0022

0.0005   0.0011   0.0011

Dike   0.2   0.7   1.2   1.7   x (m)

Mixing Length Model

0.0005   0.0005

0.0011

0.0017   0.0011

0.0005

Standard k-ε Model

0.0005
0.0017   0.0022

Non-equilibrium k-ε Model

0.0005   0.0011   0.0017

RNG k-ε Model

0.0005   0.0011   0.0017
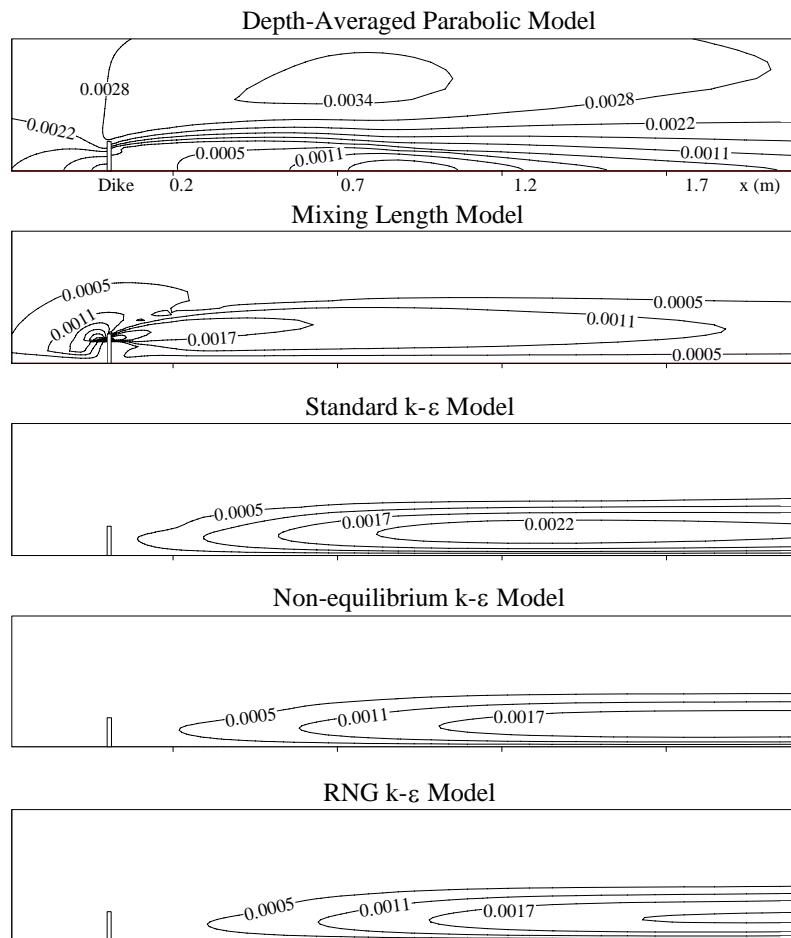
Fig. 4 Calculated Viscosities around a Spur-Dyke

15
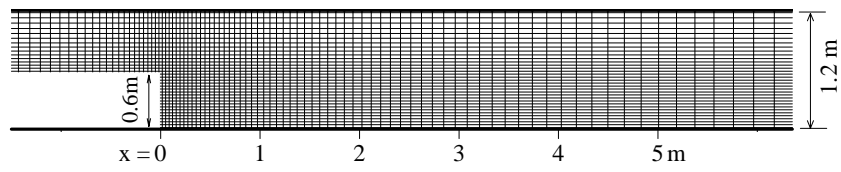
Fig. 5 Computational Mesh in the Sudden-Expanded Flume
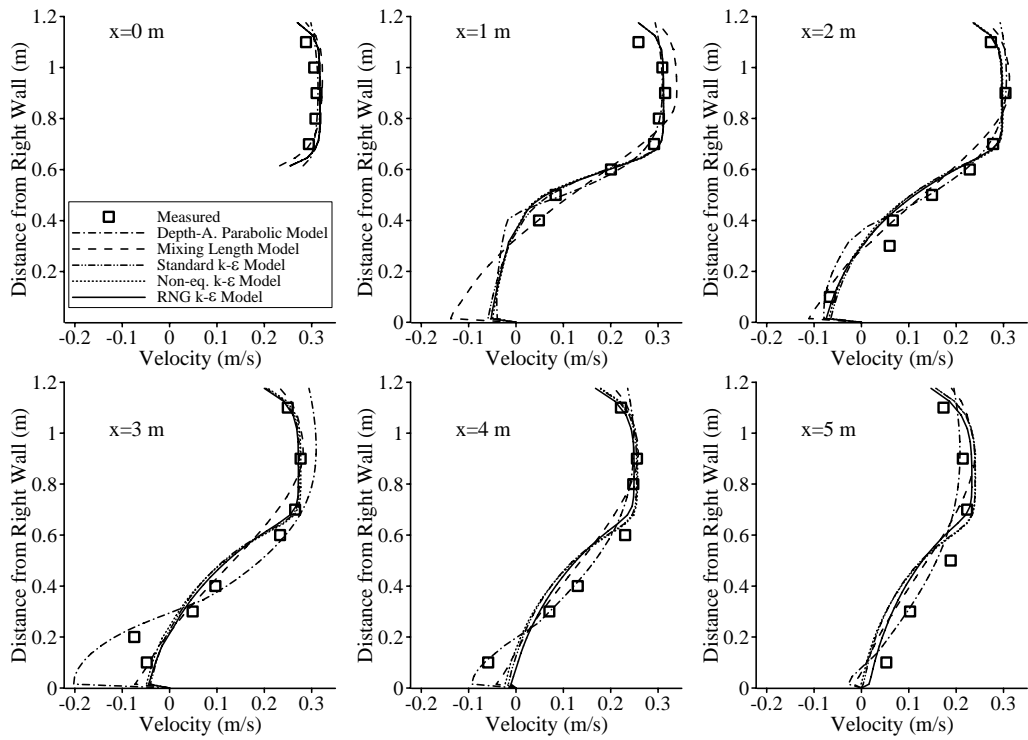
Fig. 6 Measured vs. Calculated Velocities in the Sudden-Expanded Flume
(Q=0.01815 m^3/s)
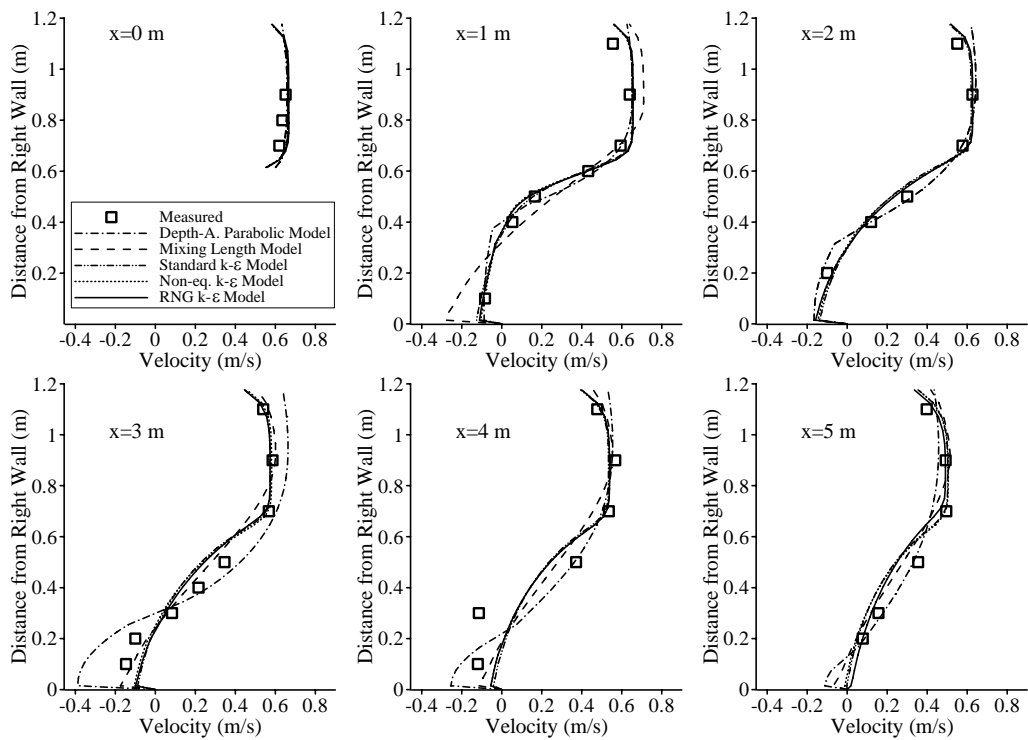
Fig. 7 Measured vs. Calculated Velocities in the Sudden-Expanded Flume
(Q=0.03854 m^3/s)
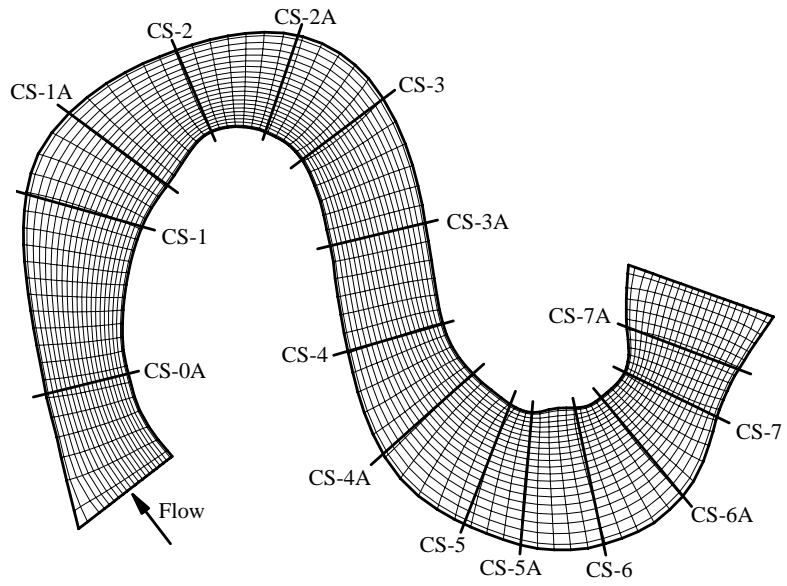
Fig. 8 Computational Mesh (Coarse) in the Study Reach of the Fall River
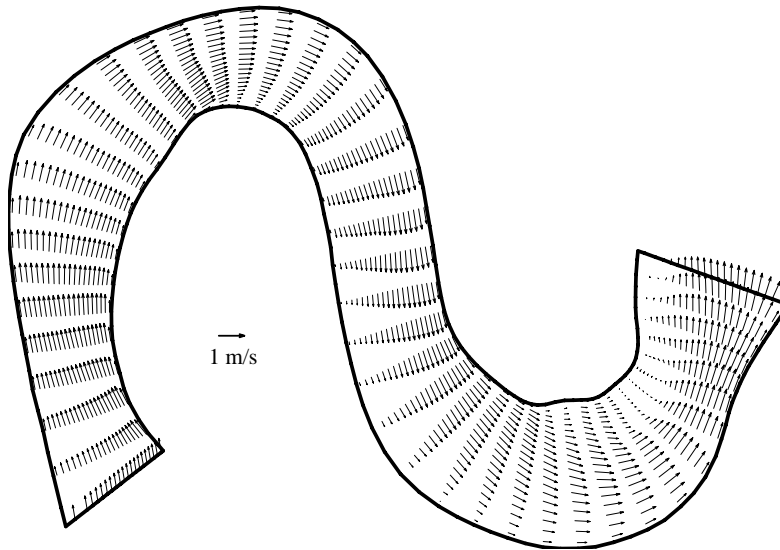
Fig. 9 Flow Field in the Fall River Calculated by using Standard k-ε Model
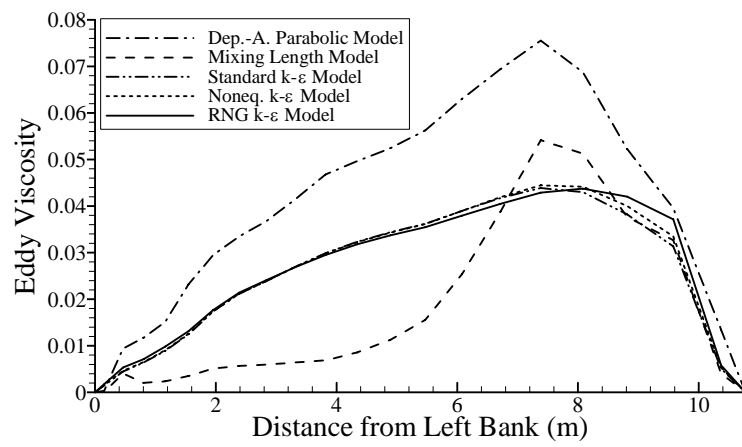
Fig. 10 Calculated Eddy Viscosities in CS-5A
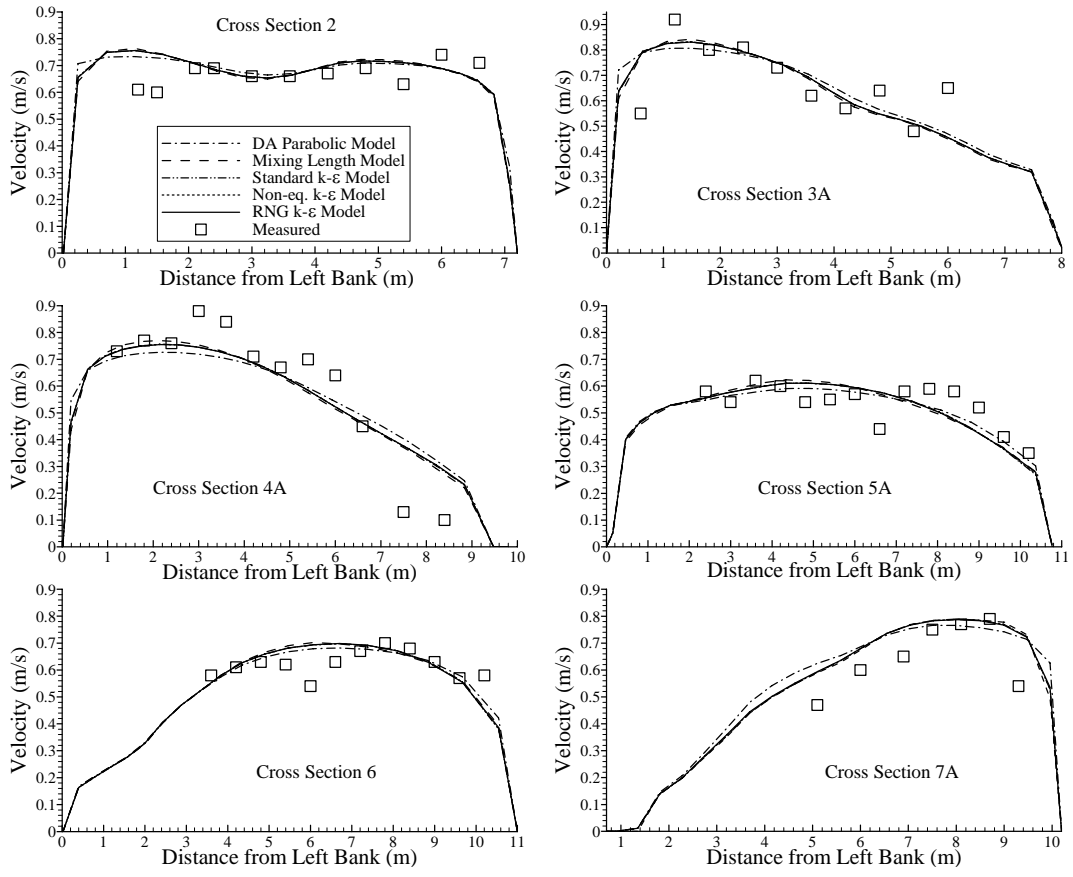
Fig. 11 Measured vs. Calculated Velocity in the Fall River
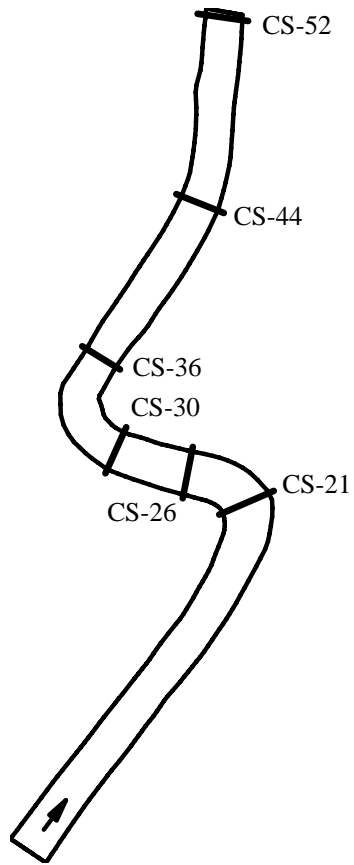
Fig. 12 Sketch of the Study Reach of the Dommel River
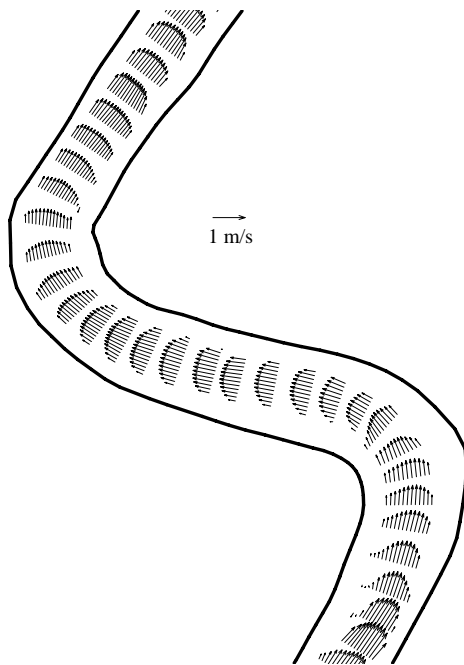
Fig. 13 Calculated Flow Field in part of the Dommel River
(Standard k-ε Model)
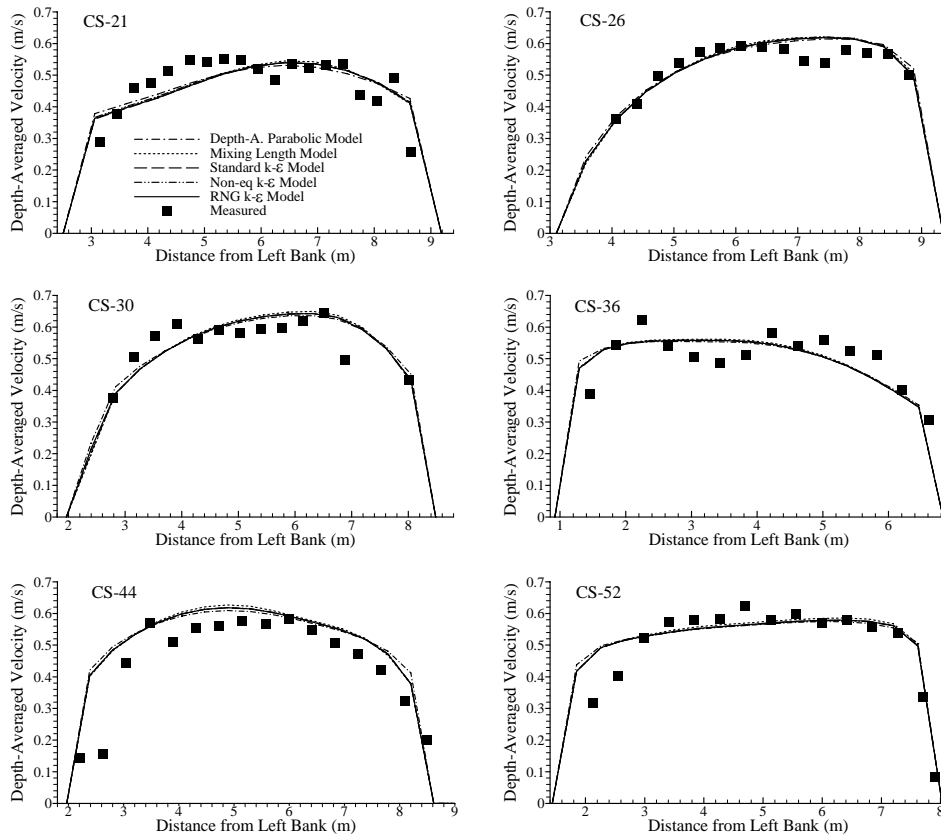
Fig. 14 Measured vs. Calculated Velocities in the Dommel River